crystals

MDPI

Article

Rapid and Selective Sensing of 2,4,6-Trinitrophenol via a Nano-Plate Zn(II)-Based MOF Synthesized by Ultrasound Irradiation

Xiao-Wei Yan [1], Azar Hakimifar [2], Fahime Bigdeli [2], Younes Hanifehpour [3], Su-Juan Wang [1,*], Kuan-Guan Liu [4], Ali Morsali [2,*] and Sang Woo Joo [5,*]

1 Guangxi Key Laboratory of Health Care Food Science and Technology, College of Food and Bioengineering, Hezhou University, No. 18 West Ring Road, Hezhou 542899, China; yanxiaoweizb@163.com
2 Department of Chemistry, Faculty of Sciences, Tarbiat Modares University, Tehran P.O. Box 14115-4838, Iran; hakimifar.azar2004@gmail.com (A.H.); bigdeli.fahimeh@gmail.com (F.B.)
3 Department of Chemistry, Sayyed Jamaleddin Asadabadi University, Asadabad 6541861841, Iran; younes.hanifehpour@gmail.com
4 Ningxia Key Laboratory for Photovoltaic Materials, Ningxia University, Yinchuan 750021, China; liukuanguan@nxu.edu.cn
5 School of Mechanical Engineering, Yeungnam University, Gyeongsan 712-749, Republic of Korea
* Correspondence: bemyselfwsj@yeah.net (S.-J.W.); morsali_a@modares.ac.ir (A.M.); swjoo@yu.ac.kr (S.W.J.)

Abstract: Using the sonochemical method, nano-plates of a 3D Zn(II) metal−organic framework (MOF) were synthesized and characterized using FT-IR spectroscopy and PXRD. The effect of various irradiation durations and concentrations of reagents was investigated to obtain uniform morphologies. Increasing the irradiation time along with decreasing the reagent concentration led to the production the particles with a uniform nano-plate morphology. Also, the sensing potential of these nano-plates to detect nitroaromatic analytes such as nitrophenol, 2,4-dinitrophenol, and TNP was explored. The nano Zn MOF was highly selective and sensitive in the detection of nitroaromatic derivatives. The quenching percentages of fluorescence emissions for a 2ppb concentration of nitrophenol, 2,4-dinitrophenol, and TNP were 11%, 42%, and 89%, respectively. According to the results, the MOF has the strongest detection limit for TNP.

Keywords: MOF; nanostructure; ultrasound; fluorescence; nitroaromatic

check for updates

Citation: Yan, X.-W.; Hakimifar, A.; Bigdeli, F.; Hanifehpour, Y.; Wang, S.-J.; Liu, K.-G.; Morsali, A.; Joo, S.W. Rapid and Selective Sensing of 2,4,6-Trinitrophenol via a Nano-Plate Zn(II)-Based MOF Synthesized by Ultrasound Irradiation. *Crystals* **2023**, *13*, 1344. https://doi.org/10.3390/cryst13091344

Academic Editors: Linda J.W. Shimon, Saied M. Soliman, Assem Barakat and Ayman El-Faham

Received: 7 July 2023
Revised: 11 August 2023
Accepted: 23 August 2023
Published: 3 September 2023

Copyright: © 2023 by the authors. Licensee MDPI, Basel, Switzerland. This article is an open access article distributed under the terms and conditions of the Creative Commons Attribution (CC BY) license (https://creativecommons.org/licenses/by/4.0/).

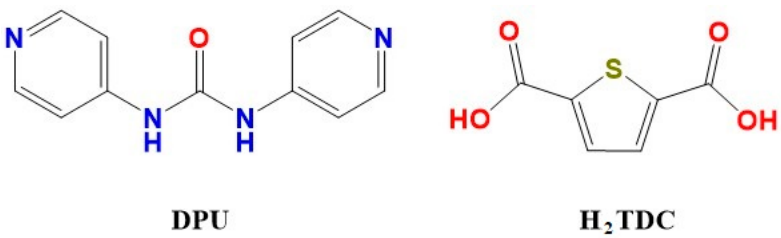
1. Introduction

In the last decade, MOFs have attracted a great deal of consideration due to their potential in many applications such as gas separation and storage, catalysis, and sensing [1–3]. This interest is relying on their intrinsic high porosity coupled with their stability and functionality achieved by the rational selection of the network structural units [4–7]. Recently, many efforts have been made to invent new synthetic methods to control the size and morphology of MOFs [8,9]. Different morphologies such as nanospheres, nanorods, nano-plates, and nanotubes in MOF nanostructures can influence their chemical and physical properties, leading to many potential applications [10–12]. Ultrasound has become common with the development of the synthesis of various materials and engineering in recent years.

Sonochemical synthesis is one of the easy methods to prepare nano and bulk materials. This synthesis takes less than an hour, while methods such as solvothermal often require a duration of 48 h for synthesis. In addition, the particles formed by the sonochemical process are much smaller than those produced by conventional syntheses [13]. In addition to the production of nanoparticles, ultrasound radiation can provide necessary energy to create covalent interactions between particles to facilitate the formation of composites [14]. Over the past decade, ultrasonic synthesis has been recognized as a powerful method in the synthesis of MOFs, widely used in recent years to build nanoparticles with particular

morphologies [15,16]. Ultrasonic chemical effects do not result from direct interaction with chemical species at the molecular level. Sonochemical performance is related to the energy released by acoustic cavitation. When liquids collide with a high energy ultrasound generator, sonic cavitation arises through shock waves generated in the medium. Bubbles are formed and gradually become bigger; with their destruction, high pressure (up to 1000 atm) and high temperature (up to 5000 K) are created in the environment [17].

Ultrasound is a cost-effective, mild, reproducible, and environmentally friendly technique for the preparation of nanomaterials with interesting morphologies and new features [18–23]. Ultrasound can be strong enough to cause dissolution, hydrolysis, and decomposition [13]. However, some parameters such as the ultrasonic output power, solvent nature, and the temperature of the solution affect the efficiency of ultrasound [24]. Ultrasound is one of the best techniques for the synthesis of MOFs at nano/micro-scales with attractive particle sizes and morphologies and improved performance [25–31]. We reviewed the synthesis of nanoMOFs using the ultrasonic method [32]. The first nanoMOF synthesized using an ultrasonic technique was reported by Qiu et al. They prepared nanocrystals of $Zn_3(BTC)_2{\cdot}12H_2O$ as a fluorescent microporous MOF using an ultrasound frequency of 40 KHz (60 W) at room temperature and with a reaction time of 5–90 min [33]. In another example, our group's report demonstrated that nano TMU-40 synthesized using the ultrasonic method showed better sensitivity than that in bulk TMU-40 due to the effective interaction between the analyte molecules and nano MOF [26]. In recent years, MOFs have been used for the selective detection and absorption of toxic compounds, such as nitroaromatic compounds (NACs), explosives, anions, and cations [34–41]. The selective detection and elimination of NAC explosives is a global problem due to the pollution of soil and groundwater, as well as other applications related to their high toxicity and explosive nature [42,43]. Nanosized MOFs possess a better performance than the bulk phase in applications such as sensing because they provide a short transport path for guest molecules due to their high surface area, which leads to easy access to the active sites [26]. Sensing and absorbing volatile organic compounds (VOCs) is very important in terms of safety and environmental health aspects [44]. VOCs are toxic compounds, and some of them have harmful consequences for human health even at concentrations as low as ppb. Therefore, controlling their spread in the ecosystem is important to maintain the health of living organisms, and it is necessary to find easy and efficient methods [45,46]. Conventional techniques such as chromatography, nuclear magnetic resonance, mass spectrometry, etc., have been developed to separate VOCs, but they may have some disadvantages such as a high cost and lack of portability. Also, these techniques usually require complex and time-consuming pretreatment steps and highly skilled operators [47]. Therefore, the synthesis of new sensors for the detection and separation of VOCs is very important not only for the removal of pollutants but also for the advancement of analytical and material sciences [48]. The effective and selective sensing of NACs such as 2,4-dinitrophenol (2,4-DNP) and 2,4,6-trinitrophenol (TNP) is the subject of the present study [49]. It has been argued that the aromatic ligands in the MOFs play a significant role in the interaction with NACs through π interactions, specifically π-π stacking and C-H$\cdots\pi$ interactions [50]. In this work, the 1,3-di(pyridin-4-yl)urea (DPU) ligand and thiophene-2,5-dicarboxylic acid (H_2TDC) ligand (Scheme 1) has been used to prepare a new Zn(II)-based MOF, [Zn(TDC)(DPU)].0.85DMF] (TMU-57).



DPU **H_2TDC**

Scheme 1. Scheme of used ligands for preparation of the nano-plates of MOF TMU-57.

The presence of a Lewis basic urea function in DPU ligand and thiophene as a sulfur function in TDC^{2-} linker as a bifunctional compound has the ability to interact with nitrophenol compounds via donor–acceptor interactions and hydrogen bonding. Sonochemical reactions were considered for preparing this structure. Moreover, TMU-57 was synthesized using the ultrasound method, and the effect of reagent concentrations and power of the ultrasonic device on the size and shape of the products was studied. Also, the fluorescence property of TMU-57 nano-plates was investigated against different nitroaromatic analytes.

2. Experimental Section

2.1. Materials and Measurements

The materials for synthesis were purchased from commercial centers and used without further purification (Sigma-Aldrich, Merck and the others). The IR spectra (in KBr pellets) were carried out on a Nicolet Fourier Transform IR (Thermo Fisher Scientific Company, MA, US), Nicolet 100 spectrometer in the range 400–4000 cm^{-1}. The X-ray powder diffraction (XRD) (Philips Company, Amsterdam, The Netherlands) measurements were obtained by a Philips X'pert diffractometer with monochromated Cu-kα radiation (λ = 1.54056 Å). SONICA-2200 EP with an adjustable power output (maximum 305 W at 40/60 kHz) was applied as a sonicator. A tubular pyrex reactor was prepared and connected to the sonicator bath. The simulated XRD powder pattern was obtained by single-crystal data using the Mercury software.

2.2. Synthesis of TMU-57 Nanostructures

For the synthesis of nano-sized TMU-57, $Zn(CH_3COO)_2{\cdot}2H_2O$ (0.065 g, 0.5 mmol), H_2TDC (0.107 g, 0.5 mmol), and 1,3-di(pyridin-4-yl)urea (L) (0.086 g, 0.5mmol) were added to 10 mL of DMF and placed in high-density ultrasonic equipment, with a power output of 305 W, at room temperature, and sonicated for 60 min. The white powder as a product was separated from the solution by centrifugation, washed with DMF, and then dried at 80 °C. For the activation, the product was immersed in dichloromethane for 2 days and refreshed once daily. Then, it was heated to 100 °C for 12 h to remove solvent molecules from the TMU-57 pores. IR data (KBr pellet, m/cm^{-1}): 3341 (br), 1675 (vs), 1592 (vs), 1525 (vs), 1368 (s), 1293 (m), 1193 (m), 907 (w), 770 (m), 658 (w), and 530 (w). Sensing reactions were carried out with several concentrations (0.02, 0.01, and 0.005 M) to study the effect of reagent concentrations on features of TMU-57 nanostructures.

2.3. Measurement of TMU-57 Fluorescence Properties

The fluorescence features of TMU-57 nanostructures were investigated in different solvent emulsions containing TMU-57. Briefly, 1 mg of an activated TMU-57 was milled and then added to analyte solutions (2 mL); after 1 h, the fluorescence emission was measured in methanol solvent. According to the Stern–Volmer equation, $(I_0/I) = K_{SV}[A]+1$, where I_0: the initial fluorescence intensity of TMU-57 solution, I: the fluorescence intensity in the presence of analyte, [A]: the concentration of analyte (molarity), and K_{SV} is the Stern–Volmer constant (M^{-1}). To calculate the quenching constant, the emission intensity of the MOF sample was obtained for several concentrations of analyte solutions in methanol.

3. Results and Discussion

3.1. Structural Description of TMU-57

The nanostructure of a 3D MOF, [Zn(TDC)(DPU)].0.85DMF] (TMU-57), was readily synthesized via the sonochemical method. The structure of this MOF [51] shows that [Zn(TDC)(L)].0.85DMF is a three-dimensional coordination polymers with three independent Zn atoms in the framework. The disordered octahedral geometry of Zn1 atom includes three O atoms belonging to two TDC^{2-} atoms and two pridyl N atoms of two DPU spacers. Zn2 is coordinated to three oxygen atoms related to two carboxylic ligands, two nitrogen atoms of two L, and also one oxygen atom that is bridged to Zn3. Therefore, Zn centers form a three-dimensional structure by two bonds with TDC^{2-} in the equatorial position

and two DPU ligands through their pyridyl groups in the axial position (Figure 1). The details of the crystallographic data are listed in Table 1 [51].

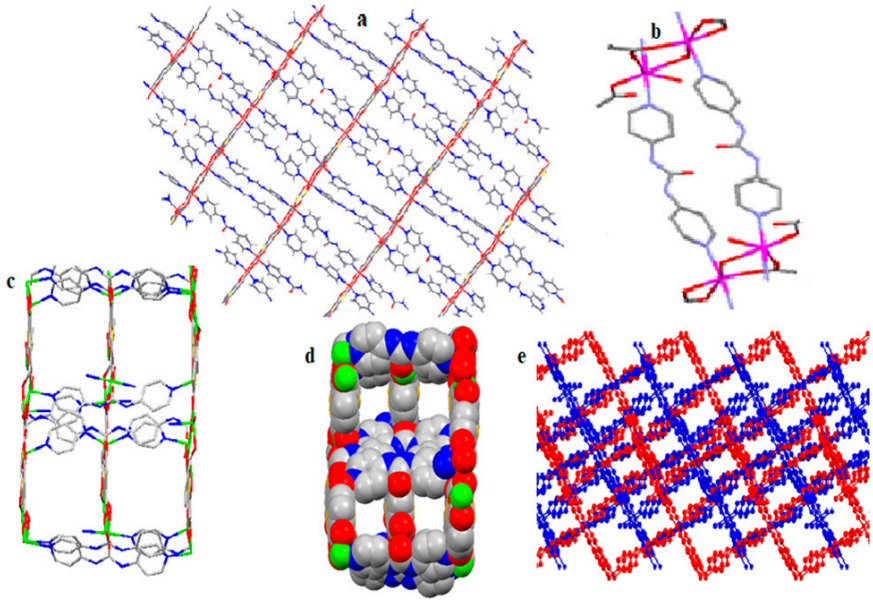


Figure 1. Crystal structure of TMU-57: (**a**) 3D layers of Zn(II)-tdc unit pillared by the urea ligand; (**b**) coordination geometry around Zn metal center; (**c**) schematic representation of the structure; (**d**) spacefill representation of binuclear Zn2 unit (color code: Zn: green; O: red; N: blue; C: gray). (**e**) The two interpenetrating frameworks are shown in red and blue.

Table 1. Structural data and refinement parameters for TMU-57.

Identification Code	TMU-57
CCDC number	1,908,579
Formula	$C_{51}H_{36}N_{12}O_{15}S_3Zn_3$,2.55 ($C_3H_7NO$)
Fw	1535.61
T/K	293 (2)
crystal system	monoclinic
space group	P21/c
a/Å	10.5925 (2)
b/Å	18.1702 (4)
c/Å	34.2901 (7)
α/°	90.0
β/°	98.665 (2)
γ/°	90.0
V/Å3	6524.4 (2)
Z	4
D_{calc}/g cm^{-3}	1.563
μ (mm^{-1})	1.272
F (000)	3144
(h k l) max	(14 24 45)
R1 (I > 2σ (I))	0.0358
wR2 (I > 2σ (I))	0.0993

3.2. Nanostructures of TMU-57

The nano-plates of this compound have been prepared via the sonochemical method in DMF solution with several concentrations (0.02, 0.01, and 0.005 M). The simulated XRD pattern of TMU-57 obtained from single-crystal X-ray data compared to the sonochemical method can be observed in Figure 2. There is a good fit between the simulated and experimental PXRD patterns, with some differences in 2θ. The particle dimensions in the nanometers range lead to broadening of the peaks. The IR spectra of nano TMU-57 obtained from the sonochemical reaction and conventional heating [51] show the band at 3341 cm $^{-1}$ ascribed to amide NH stretching vibrations. The peaks at 1193 cm^{-1} are assigned to the stretching vibration peak C=S, and the characteristic vibration peak of the C–N group appears at 1293 cm^{-1}. The band of the C=O groups was observed in the area of 1747 cm^{-1} (Figure 2—down). The vibrational peak was at 1675 cm^{-1}, which is related to the DMF molecules trapped in the TMU-57 structure, while the spectrum of the ligand does not have this peak. The thermal stability of non-activated TMU-57 was assessed, and the results clarify that 11.5% weight loss was observed in the 50−200 °C temperature range attributing to the activation of the MOF through the elimination of trapped solvent molecules inside the pores. Next, weight loss, which is observed in temperatures higher than 200 °C, relates to the decomposition of the framework (Figure 3).

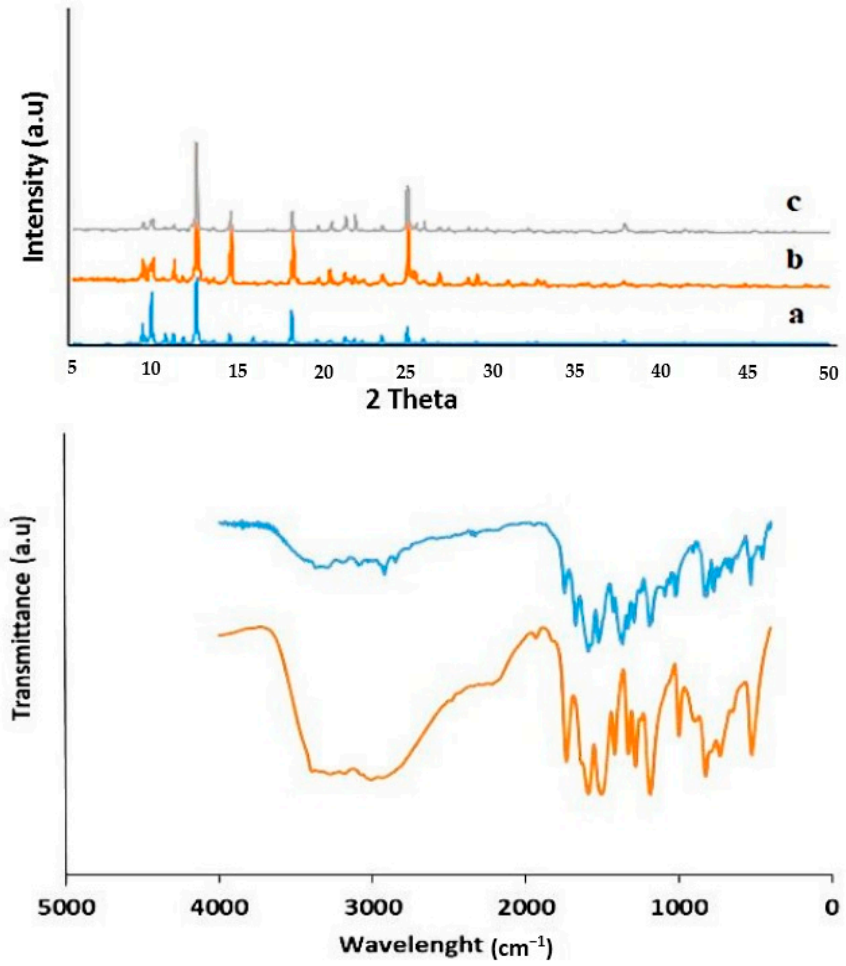


Figure 2. (**up**): PXRD patterns of simulated synthesized crystals (a), synthesized nanostructures by sonochemical (b), of TMU-57 (c); (**down**): FT-IR spectra of urea ligand (orange) and TMU-57 framework (blue). (cm^{-1}).

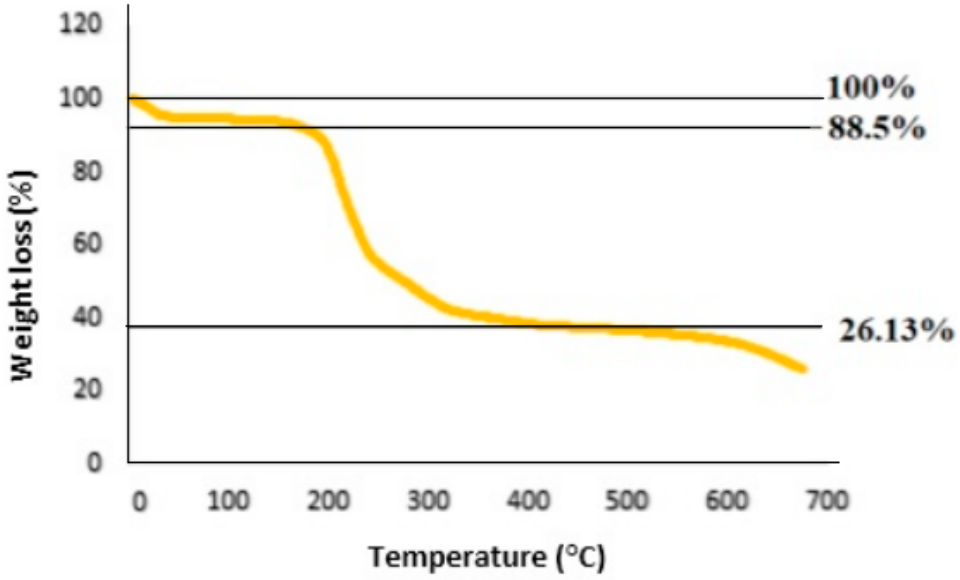


Figure 3. TGA analysis of TMU-57.

The size and morphology of TMU-57 were studied at different times and with a different initial concentration of reagents in the sonochemical reaction using scanning electron microscopy (SEM) (Philips Company, Amsterdam, The Netherlands). Sonication time (30 and 60 min) was obtained at concentrations (0.02 M, 0.01 M, and 0.005 M) (Figure 4) for TMU-57. According to the SEM images, a plate-like morphology was observed for the sonochemically prepared frameworks, and as the concentration of reactants decreases (0.01 M), the morphology becomes more uniform (Figure 5) (Table 2). Moreover, the SEM images show that nano-plates were generated in 30 min, and increasing the sonication time has the same effect on the size and morphology of the samples, but by increasing the sonication time, aggregation is reduced. Therefore, a reaction time of 60 min was selected for this MOF (Figure 5). For the synthesis of TMU-57, with the conventional solvothermal method, a reaction time of 24 h and temperature of 120 °C are required [48], while in the ultrasonic method, in a period of 30 min to 1h, at room temperature, the various and defined size and morphologies of the nanoTMU-57 product can be obtained.

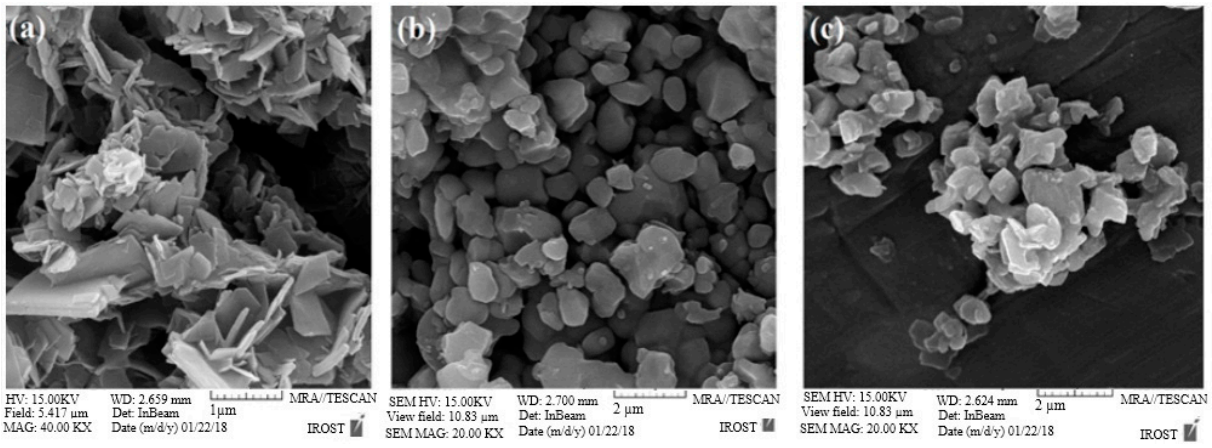


Figure 4. FE-SEM images of TMU-57 produced by different concentrations: (**a**) 0.02 M; (**b**) 0.01 M; (**c**) 0.005 M.

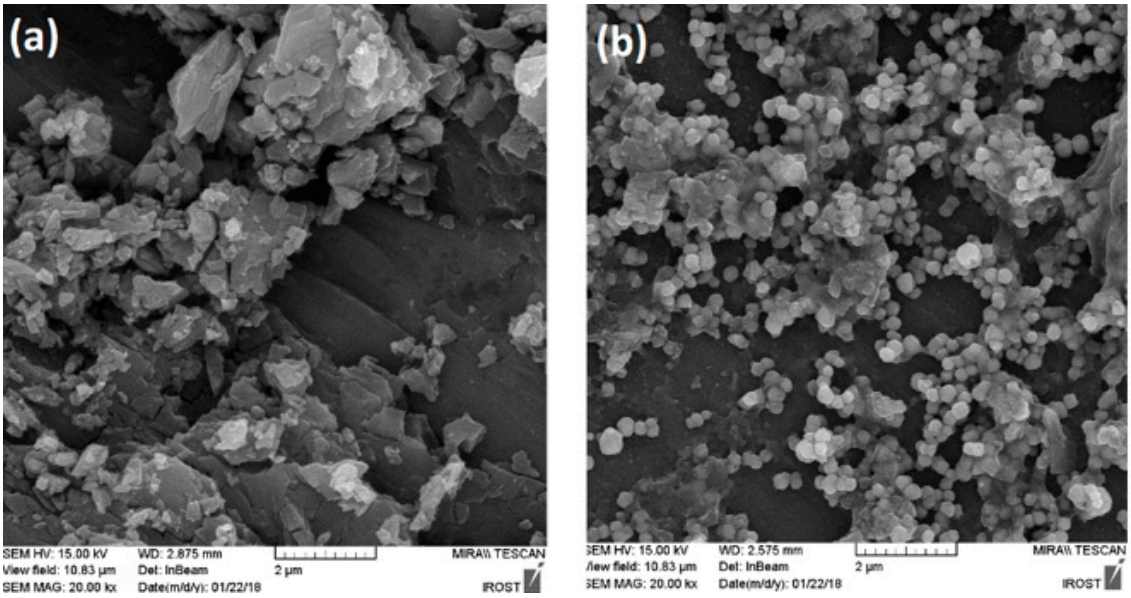


Figure 5. FE-SEM images of TMU-57 produced by different time: (**a**) 30 min (0.01 M); (**b**) 1h (0.01 M).

Table 2. The effect of synthetic parameters on the features of TMU-57 nano-plates in 10 mL DMF and sonication power 305W.

Sample Name	Molar Ratio (TDC:L:$Zn(OAc)_2$) mmol	Concentration [TDC]/[L]/[$Zn(OAc)_2$] (M)	Time (min)	Morphology
A	1:1:1	[0.02]/[0.02]/[0.02]	30	Nano-plates
B	1:1:1	[0.02]/[0.02]/[0.02]	60	Nano-plates
C	1:1:1	[0.01]/[0.01]/[0.01]	30	Nano-plates
D	1:1:1	[0.01]/[0.01]/[0.01]	60	Nanoparticle
E	1:1:1	[0.005]/[0.005]/[0.005]	30	Nano-plates
F	1:1:1	[0.005]/[0.005]/[0.005]	60	Nano-plates

3.3. The Sensing Application of TMU-57 Nanostructures

To investigate the potential application of nanostructured TMU-57, for nitroaromatics (NAC) sensing, the fluorescence emission of the methanol solution of nanoTMU-57 containing analyte molecules was recorded. Then, the fluorescence signal was observed at 426 nm by excitation at 340 nm, which is ascribed to the luminescence emission excited state. The detection of nitroaromatic compounds was achieved by measuring the photoluminescence of TMU-57 nano-plates. The solutions of nitrophenol, 2,4-dinitrophenol and 2,4,6-trinitrophenol in methanol (0.2 M) were separately added to 2mL of methanol solution of Nano TMU-57.

The reduction in the fluorescence intensity of Nano-MOF TMU-57 with an increasing concentration of nitroaromatic compound solutions indicates efficient quenching effects (Figure 6a–c). Upon excitation, electrons are transferred from the conduction band of TMU-57 to the LUMO of the nitrophenol compounds as the electron deficient analyte, leading to the quenching effect of the TMU-57 [52].

The Stern–Volmer constant (Ksv) is one of the significant parameters to evaluate the efficiency of the sensors in detecting analyte molecules. The Stern–Volmer equation is as follows: $I_0/I = Ksv[CM] + 1$, where I_0 is the PL emission intensities in the absence of NACs, and I is PL emission intensities in the presence of NACs. Ksv and CM represent the Stern–Volmer constant in $L.mol^{-1}$ and the concentration of the NAC molecules. The quenching efficiency for nitroaromatic sensing was evaluated using the Stern–Volmer equation for

TMU-57 (Figure 7). TNP (Ksv = 2×10^6 M^{-1}) shows the highest Ksv, which indicates the selectivity for TNP by this MOF (Figure 8). These results reveal that TMU-57 nano-plate has sufficient sensitivity to detect nitroaromatic explosives easily, rapidly, and via the green chemistry method. Among these, the structure is mostly in response to TNP, and the quenching efficiency for 2,4,6-trinitrophenol (TNP) is higher than 2,4-dinitrophenol(DNP) and, respectively, higher than 4-nitrophenol(NP) (Figure 9). The quenching percentages of fluorescence emission intensity in the presence of 2 ppb of nitrophenol, 2,4-dinitrophenol, and TNP were 11%, 42%, and 89%, respectively (Figure 9). Examining the reports related to the sensing of nitrophenol compounds shows that the concentration of analyte molecules that can be detected by nanoTMU-57 is relatively low (2 ppb), and this MOF shows the excellent detection limit and selectivity [53–58]. The TMU-57 performance in the bulk phase was reported by our group. These results confirmed that TMU-57 MOF has good potential for sensing explosives such as TNP. The presence of the Lewis basic urea function in DPU ligand and thiophene as a sulfur function in TDC^{2-} linker as a bifunctional compound has the ability to interact with nitrophenol compounds via donor–acceptor interactions and hydrogen bonding [23,59]. For the fluorescence sensing of TMU-57, upon excitation, electrons are transferred from the conduction band of TMU-57 to the LUMO of the nitrophenol compounds as the electron deficient analyte, leading to a quenching effect of the TMU-57 [52].

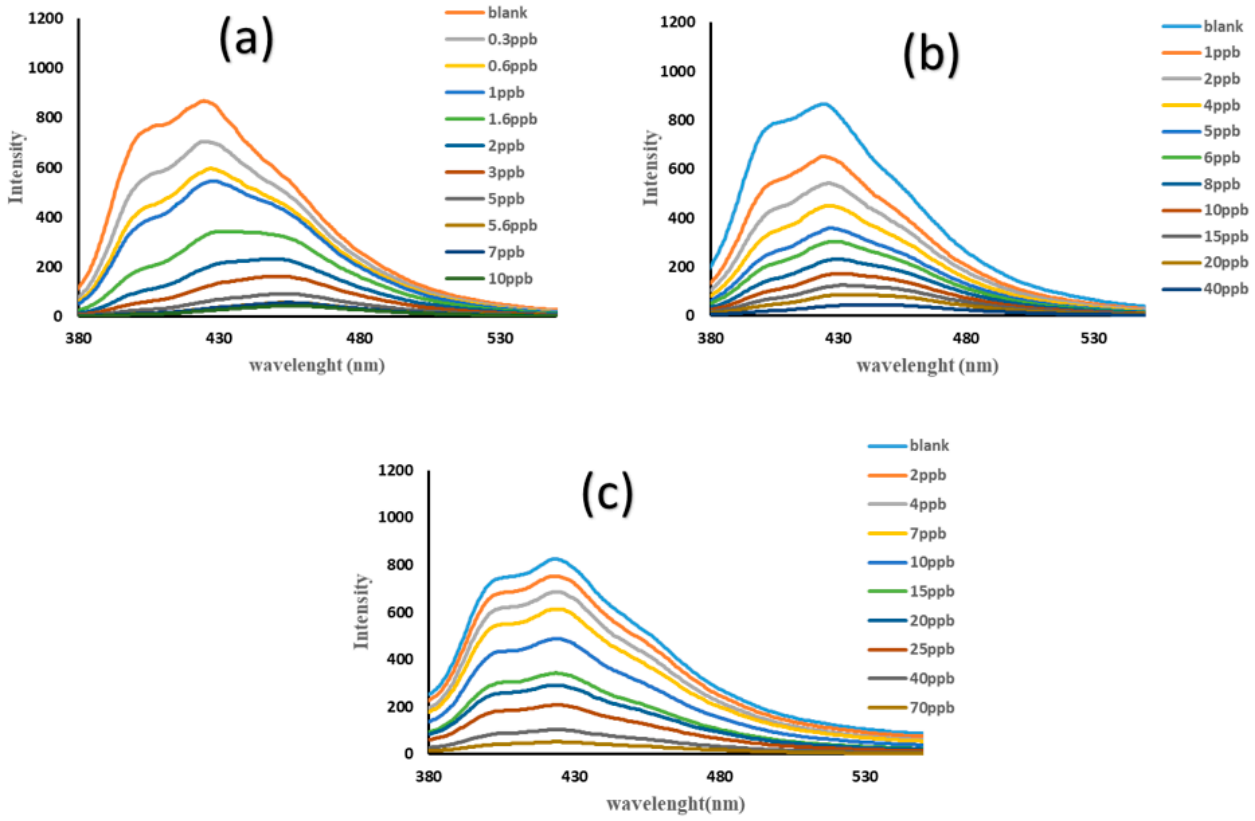


Figure 6. Change in fluorescence emission of NMOF with different concentrations of nitroaromatic compounds: (**a**) 2,4,6-trinitrophenol; (**b**) 2,4-dinitrophenol; (**c**) 4-nitrophenol in 2 mL methanol. With excitation at 340 nm and investigation of the fluorescence emission from 380 nm to 530 nm.

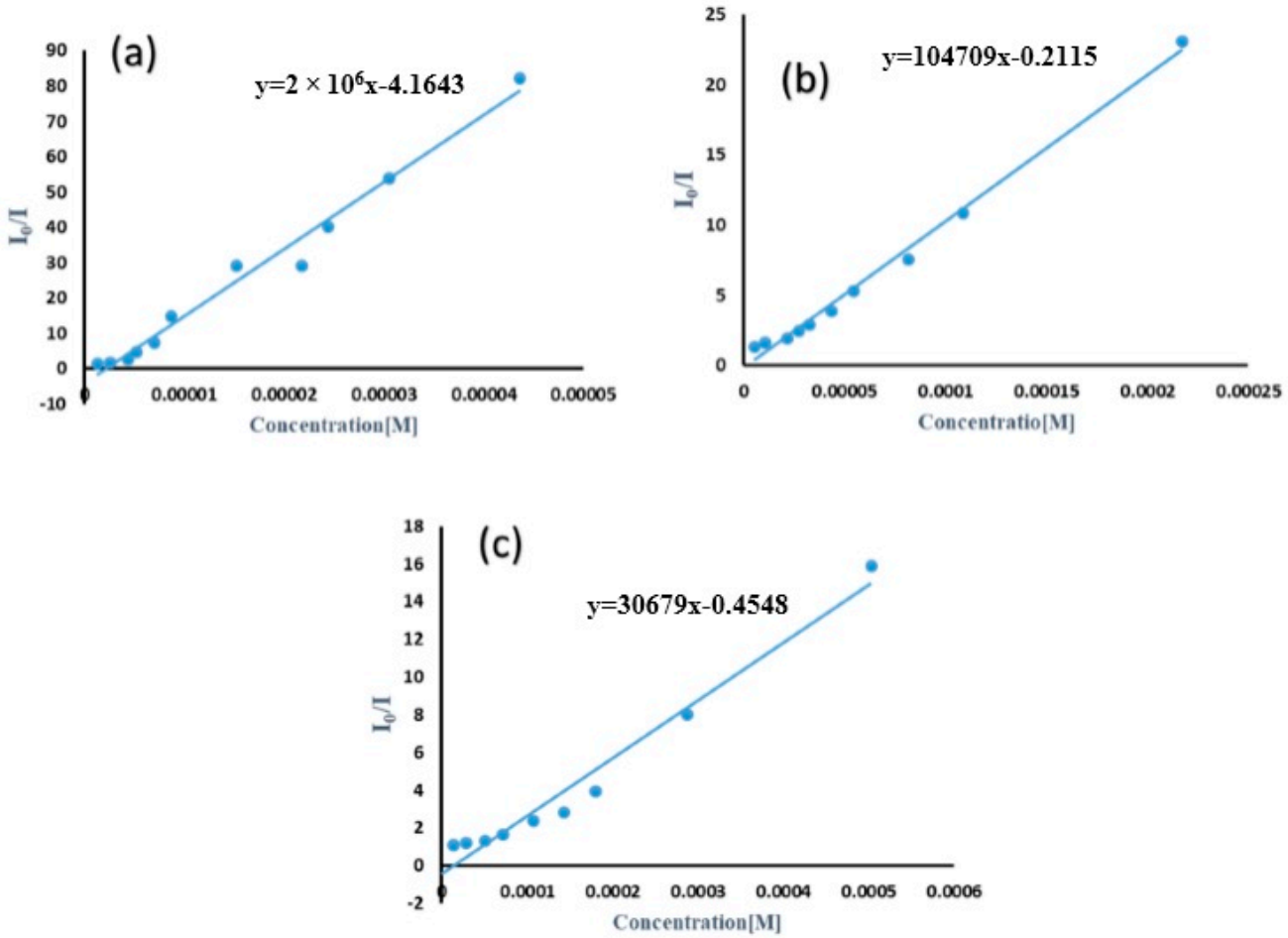


Figure 7. K_{SV} plots of nitroaromatic compounds in methanol; (**a**) TNP, (**b**) DNP, (**c**) NP.

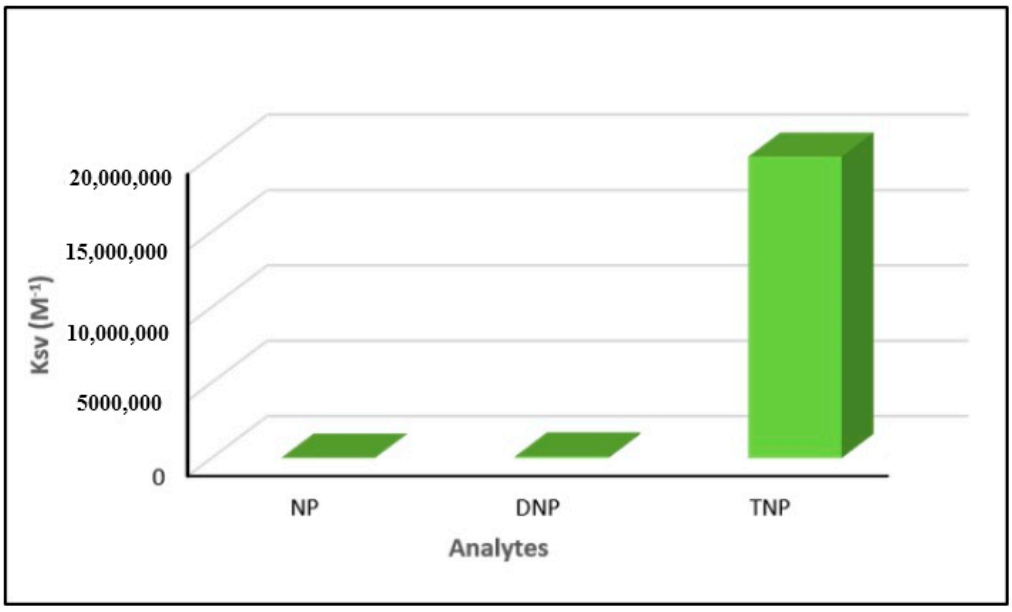


Figure 8. Comparison of K_{SV} of TMU-57 against nitroaromatic compounds (NACs).

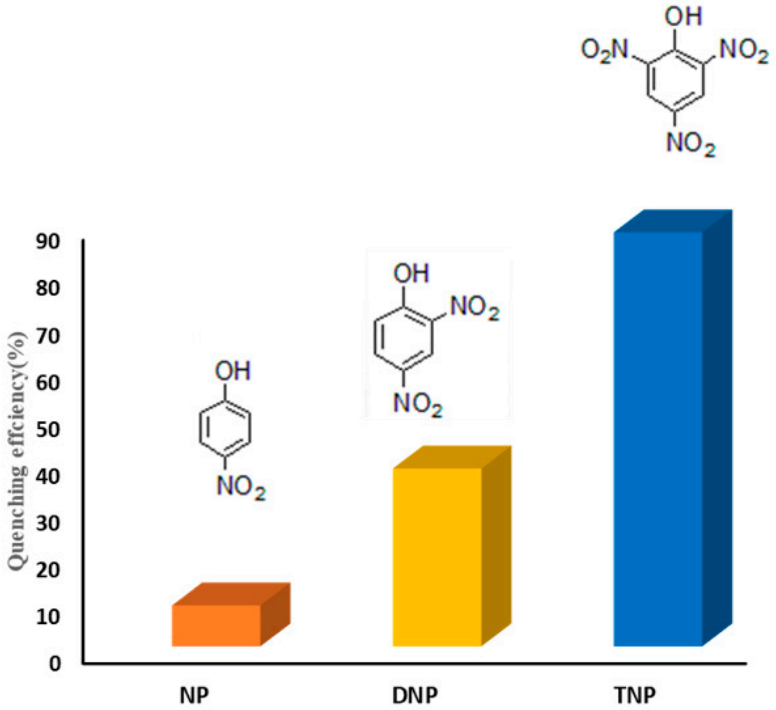


Figure 9. Comparison of quenching percent of TMU-57 fluorescence to 2 ppb of different organics in methanol solution at room temperature.

4. Conclusions

Nanostructured MOF TMU-57 was synthesized using a sonochemical method and characterized via IR spectroscopy, XRD, and SEM. The effects of various parameters like irradiation times and different initial reagents concentrations were tested. According to the results, nano-plate morphology was obtained in a 0.01 M concentration with 305 W, and an increase in the ultrasound irradiation time led to the formation of smaller particles. The study of nitroaromatics (NAC) sensing using a fluorescence measurement was performed with the addition of analytes to the methanol solution of TMU-57 nano-plates. The results show that the nano-plates of TMU-57 act as an effective sensor for TNP-like organic explosive materials due to excellent fluorescence sensing and selective probe for TNP. Therefore, multifunctional MOFs can combine sensitization and optical sensing properties which introduce them as useful candidates for sensing applications.

Nanomaterials as sensors show a better performance than their bulk phase because analyte molecules traverse a short transport route within the nanostructure with a higher surface area, which results in easy access to the active sites. The ultrasonic method is one of the easiest and most effective methods for preparing nanomaterials with uniform sizes and defined morphologies. Nanomaterials with new features can be produced to improve potential applications by changing parameters such as the concentration of reactants, time and temperature reaction, or the power of the ultrasonic device.

Author Contributions: X.-W.Y.: writing—review and editing; A.H.: writing—original draft preparation; F.B.: writing—review and editing; Y.H.: writing—review and editing; S.-J.W.: supervision, writing—review and editing; K.-G.L.: formal analysis; A.M.: supervision, writing—review and editing; S.W.J.: project administration and editing. All authors have read and agreed to the published version of the manuscript.

Funding: Financial support of this research by Tarbiat Modares University and the Middle-aged and Young Teachers' Basic Ability Promotion Project of Guangxi (2021KY0702) are gratefully acknowledged. This work was funded by 2022 Yeungnam University Grant.

Institutional Review Board Statement: Not applicable.

Informed Consent Statement: Not applicable.

Data Availability Statement: Data is contained within the article.

Conflicts of Interest: The authors declare no conflict of interest.

References

1. Xu, H.; Li, Y.; Luo, X.; Xu, Z.; Ge, J. Monodispersed gold nanoparticles supported on a zirconium-based porous metal–organic framework and their high catalytic ability for the reverse water–gas shift reaction. *Chem. Commun.* **2017**, *53*, 7953–7956. [CrossRef] [PubMed]
2. Li, B.; Wang, H.; Chen, B. Microporous Metal–Organic Frameworks for Gas Separation. *Chem. Asian J.* **2014**, *9*, 1474–1498. [CrossRef]
3. Hao, S.Y.; Ma, X.G.; Cui, G.H. Ultrasonic synthesis of two nanostructured cadmium(II) coordination supramolecular polymers: Solvent influence, luminescence and photocatalytic properties. *Ultrason. Sonochem.* **2017**, *37*, 414–423. [CrossRef]
4. Li, P.; Moon, S.-Y.; Guelta, M.A.; Harvey, S.P.; Hupp, J.T.; Farha, O.K. Encapsulation of a nerve agent detoxifying enzyme by a mesoporous zirconium metal–organic framework engenders thermal and long-term stability. *J. Am. Chem. Soc.* **2016**, *138*, 8052–8055. [CrossRef] [PubMed]
5. Furukawa, H.; Gándara, F.; Zhang, Y.-B.; Jiang, J.; Queen, W.L.; Hudson, M.R.; Yaghi, O.M. Water Adsorption in Porous Metal–Organic Frameworks and Related Materials. *J. Am. Chem. Soc.* **2014**, *136*, 4369–4381. [CrossRef] [PubMed]
6. Zhao, M.; Ou, S.; Wu, C.-D. Porous metal–organic frameworks for heterogeneous biomimetic catalysis. *Acc. Chem. Res.* **2014**, *47*, 1199–1207. [CrossRef]
7. Mogale, R.; Conradie, J.; Langner, E.H. Trans–cis kinetic study of azobenzene-4, 4′-dicarboxylic acid and aluminium and zirconium based azobenzene-4, 4′-dicarboxylate MOFs. *Molecules* **2022**, *27*, 1370. [CrossRef] [PubMed]
8. Mu, J.; Zhong, X.; Dai, W.; Pei, X.; Sun, J.; Zhang, J.; Luo, W.; Zhou, W. Metal-Organic Framework Assembled on Oriented Nanofiber Arrays for Field-Effect Transistor and Gas Sensor-Based Applications. *Molecules* **2022**, *27*, 2131. [CrossRef]
9. Li, P.; Klet, R.C.; Moon, S.-Y.; Wang, T.C.; Deria, P.; Peters, A.W.; Klahr, B.M.; Park, H.-J.; Al-Juaid, S.S.; Hupp, J.T. Synthesis of nanocrystals of Zr-based metal–organic frameworks with csq-net: Significant enhancement in the degradation of a nerve agent simulant. *Chem. Commun.* **2015**, *51*, 10925–10928. [CrossRef]
10. D'Agata, A.; Fasulo, S.; Dallas, L.J.; Fisher, A.S.; Maisano, M.; Readman, J.W.; Jha, A.N. Enhanced toxicity of 'bulk'titanium dioxide compared to 'fresh'and 'aged'nano-TiO_2 in marine mussels (Mytilus galloprovincialis). *Nanotoxicology* **2014**, *8*, 549–558. [CrossRef]
11. Soltanzadeh, N.; Morsali, A. Sonochemical synthesis of a new nano-structures bismuth(III) supramolecular compound: New precursor for the preparation of bismuth(III) oxide nano-rods and bismuth(III) iodide nano-wires. *Ultrason. Sonochem.* **2010**, *17*, 139–144. [CrossRef] [PubMed]
12. Mautschke, H.H.; Llabrés i Xamena, F.X. MOF-808 as a Highly Active Catalyst for the Diastereoselective Reduction of Substituted Cyclohexanones. *Molecules* **2022**, *27*, 6315. [CrossRef] [PubMed]
13. Ali Dheyab, M.; Aziz, A.A.; Jameel, M.S. Recent advances in inorganic nanomaterials synthesis using sonochemistry: A comprehensive review on iron oxide, gold and iron oxide coated gold nanoparticles. *Molecules* **2021**, *26*, 2453. [CrossRef]
14. Jameel, M.S.; Aziz, A.A.; Dheyab, M.A.; Mehrdel, B.; Khaniabadi, P.M. Rapid sonochemically-assisted green synthesis of highly stable and biocompatible platinum nanoparticles. *Surf. Interfaces* **2020**, *20*, 100635. [CrossRef]
15. Joharian, M.; Morsali, A. Ultrasound-assisted synthesis of two new fluorinated metal-organic frameworks (F-MOFs) with the high surface area to improve the catalytic activity. *J. Solid State Chem.* **2019**, *270*, 135–146. [CrossRef]
16. Joharian, M.; Abedi, S.; Morsali, A. Sonochemical synthesis and structural characterization of a new nanostructured Co (II) supramolecular coordination polymer with Lewis base sites as a new catalyst for Knoevenagel condensation. *Ultrason. Sonochem.* **2017**, *39*, 897–907. [CrossRef] [PubMed]
17. Negishi, K. Experimental studies on sonoluminescence and ultrasonic cavitation. *J. Phys. Soc. Jpn.* **1961**, *16*, 1450–1465. [CrossRef]
18. Ma, D.; Li, B.; Zhou, X.; Zhou, Q.; Liu, K.; Zeng, G.; Li, G.; Shi, Z.; Feng, S. A dual functional MOF as a luminescent sensor for quantitatively detecting the concentration of nitrobenzene and temperature. *Chem. Commun.* **2013**, *49*, 8964–8966. [CrossRef]
19. Sadeghzadeh, H.; Morsali, A.; Retailleau, P. Ultrasonic-assisted synthesis of two new nano-structured 3D lead(II) coordination polymers: Precursors for preparation of PbO nano-structures. *Polyhedron* **2010**, *29*, 925–933. [CrossRef]
20. Fard-Jahromi, M.J.S.; Morsali, A. Sonochemical synthesis of nanoscale mixed-ligands lead(II) coordination polymers as precursors for preparation of $Pb_2(SO_4)O$ and PbO nanoparticles; thermal, structural and X-ray powder diffraction studies. *Ultrason. Sonochem.* **2010**, *17*, 435–440. [CrossRef]
21. Nur Atiqah, S. *Design and Fabrication of Solar Light Responsive New Metal Organic Frameworks for Photocatalysis/Nur Atiqah Surib*; University of Malaya: Kuala Lumpur, Malaya, 2018.
22. Abbasi, A.R.; Morsali, A. Syntheses and characterization of AgI nano-structures by ultrasonic method: Different morphologies under different conditions. *Ultrason. Sonochem.* **2010**, *17*, 572–578. [CrossRef] [PubMed]
23. Hakimifar, A.; Morsali, A. High-sensitivity detection of nitroaromatic compounds (NACs) by the pillared-layer metal-organic framework synthesized via ultrasonic method. *Ultrason. Sonochem.* **2019**, *52*, 62–68. [CrossRef]
24. Dheyab, M.A.; Aziz, A.A.; Jameel, M.S.; Khaniabadi, P.M.; Mehrdel, B. Sonochemical-assisted synthesis of highly stable gold nanoparticles catalyst for decoloration of methylene blue dye. *Inorg. Chem. Commun.* **2021**, *127*, 108551. [CrossRef]

25. Zarekarizi, F.; Morsali, A. Ultrasonic-assisted synthesis of nano-sized metal-organic framework; a simple method to explore selective and fast Congo Red adsorption. *Ultrason. Sonochem.* **2020**, *69*, 105246. [CrossRef] [PubMed]
26. Bigdeli, F.; Rouhani, F.; Morsali, A.; Ramazani, A. Ultrasonic-assisted synthesis of the nanostructures of a Co(II) metal organic framework as a highly sensitive fluorescence probe of phenol derivatives. *Ultrason. Sonochem.* **2020**, *62*, 104862. [CrossRef] [PubMed]
27. Vaitsis, C.; Sourkouni, G.; Argirusis, C. Metal Organic Frameworks (MOFs) and ultrasound: A review. *Ultrason. Sonochem.* **2019**, *52*, 106–119. [CrossRef]
28. Liang, J.; Zulkifli, M.Y.B.; Yong, J.; Du, Z.; Ao, Z.; Rawal, A.; Scott, J.A.; Harmer, J.R.; Wang, J.; Liang, K. Locking the Ultrasound-Induced Active Conformation of Metalloenzymes in Metal–Organic Frameworks. *J. Am. Chem. Soc.* **2022**, *144*, 17865–17875. [CrossRef]
29. Sargazi, G.; Afzali, D.; Mostafavi, A.; Ebrahimipour, S.Y. Ultrasound-assisted facile synthesis of a new tantalum(V) metal-organic framework nanostructure: Design, characterization, systematic study, and CO2 adsorption performance. *J. Solid State Chem.* **2017**, *250*, 32–48. [CrossRef]
30. Tanhaei, M.; Mahjoub, A.R.; Safarifard, V. Ultrasonic-assisted synthesis and characterization of nanocomposites from azine-decorated metal-organic framework and graphene oxide layers. *Mater. Lett.* **2018**, *227*, 318–321. [CrossRef]
31. Abazari, R.; Mahjoub, A.R. Ultrasound-assisted synthesis of Zinc(II)-based metal organic framework nanoparticles in the presence of modulator for adsorption enhancement of 2,4-dichlorophenol and amoxicillin. *Ultrason. Sonochem.* **2018**, *42*, 577–584. [CrossRef]
32. Safarifard, V.; Morsali, A. Applications of ultrasound to the synthesis of nanoscale metal–organic coordination polymers. *Coord. Chem. Rev.* **2015**, *292*, 1–14. [CrossRef]
33. Qiu, L.-G.; Li, Z.-Q.; Wu, Y.; Wang, W.; Xu, T.; Jiang, X. Facile synthesis of nanocrystals of a microporous metal–organic framework by an ultrasonic method and selective sensing of organoamines. *Chem. Commun.* **2008**, 3642–3644. [CrossRef]
34. Howarth, A.J.; Wang, T.C.; Al-Juaid, S.S.; Aziz, S.G.; Hupp, J.T.; Farha, O.K. Efficient extraction of sulfate from water using a Zr-metal–organic framework. *Dalton Trans.* **2016**, *45*, 93–97. [CrossRef] [PubMed]
35. Gole, B.; Bar, A.K.; Mukherjee, P.S. Fluorescent metal–organic framework for selective sensing of nitroaromatic explosives. *Chem. Commun.* **2011**, *47*, 12137–12139. [CrossRef]
36. Nagarkar, S.S.; Desai, A.V.; Ghosh, S.K. Engineering metal–organic frameworks for aqueous phase 2, 4, 6-trinitrophenol (TNP) sensing. *CrystEngComm* **2016**, *18*, 2994–3007. [CrossRef]
37. Yang, J.; Che, J.; Jiang, X.; Fan, Y.; Gao, D.; Bi, J.; Ning, Z. A Novel Turn-On Fluorescence Probe Based on Cu (II) Functionalized Metal–Organic Frameworks for Visual Detection of Uric Acid. *Molecules* **2022**, *27*, 4803. [CrossRef]
38. Chen, M.; Xu, W.-M.; Tian, J.-Y.; Cui, H.; Zhang, J.-X.; Liu, C.-S.; Du, M. A terbium (III) lanthanide–organic framework as a platform for a recyclable multi-responsive luminescent sensor. *J. Mater. Chem. C* **2017**, *5*, 2015–2021. [CrossRef]
39. Han, M.-L.; Wen, G.-X.; Dong, W.-W.; Zhou, Z.-H.; Wu, Y.-P.; Zhao, J.; Li, D.-S.; Ma, L.-F.; Bu, X. A heterometallic sodium–europium-cluster-based metal–organic framework as a versatile and water-stable chemosensor for antibiotics and explosives. *J. Mater. Chem. C* **2017**, *5*, 8469–8474. [CrossRef]
40. Li, B.; Jiang, Y.-Y.; Sun, Y.-Y.; Wang, Y.-J.; Han, M.-L.; Wu, Y.-P.; Ma, L.-F.; Li, D.-S. The highly selective detecting of antibiotics and support of noble metal catalysts by a multifunctional Eu-MOF. *Dalton Trans.* **2020**, *49*, 14854–14862. [CrossRef]
41. Wen, G.-X.; Han, M.-L.; Wu, X.-Q.; Wu, Y.-P.; Dong, W.-W.; Zhao, J.; Li, D.-S.; Ma, L.-F. A multi-responsive luminescent sensor based on a super-stable sandwich-type terbium (III)–organic framework. *Dalton Trans.* **2016**, *45*, 15492–15499. [CrossRef]
42. Nagarkar, S.S.; Joarder, B.; Chaudhari, A.K.; Mukherjee, S.; Ghosh, S.K. Highly selective detection of nitro explosives by a luminescent metal–organic framework. *Angew. Chem.* **2013**, *125*, 2953–2957. [CrossRef]
43. Jurcic, M.; Peveler, W.J.; Savory, C.N.; Scanlon, D.O.; Kenyon, A.J.; Parkin, I.P. The vapour phase detection of explosive markers and derivatives using two fluorescent metal–organic frameworks. *J. Mater. Chem. A* **2015**, *3*, 6351–6359. [CrossRef]
44. Ramanavicius, S.; Ramanavicius, A. Insights in the application of stoichiometric and non-stoichiometric titanium oxides for the design of sensors for the determination of gases and VOCs (TiO_{2-x} and $TinO_{2n-1}$ vs. TiO_2). *Sensors* **2020**, *20*, 6833. [CrossRef] [PubMed]
45. Monsef, R.; Ghiyasiyan-Arani, M.; Salavati-Niasari, M. Application of ultrasound-aided method for the synthesis of NdVO4 nano-photocatalyst and investigation of eliminate dye in contaminant water. *Ultrason. Sonochem.* **2018**, *42*, 201–211. [CrossRef] [PubMed]
46. Zhou, Y.; Yan, B. A responsive MOF nanocomposite for decoding volatile organic compounds. *Chem. Commun.* **2016**, *52*, 2265–2268. [CrossRef]
47. Kumar, P.; Deep, A.; Kim, K.-H.; Brown, R.J. Coordination polymers: Opportunities and challenges for monitoring volatile organic compounds. *Prog. Polym. Sci.* **2015**, *45*, 102–118. [CrossRef]
48. Zheng, J.P.; Ou, S.; Zhao, M.; Wu, C.D. A highly sensitive luminescent dye@ MOF composite for probing different volatile organic compounds. *ChemPlusChem* **2016**, *81*, 758–763. [CrossRef]
49. Sun, X.; Wang, Y.; Lei, Y. Fluorescence based explosive detection: From mechanisms to sensory materials. *Chem. Soc. Rev.* **2015**, *44*, 8019–8061. [CrossRef]
50. Hawes, C.S.; Nolvachai, Y.; Kulsing, C.; Knowles, G.P.; Chaffee, A.L.; Marriott, P.J.; Batten, S.R.; Turner, D.R. Metal–organic frameworks as stationary phases for mixed-mode separation applications. *Chem. Commun.* **2014**, *50*, 3735–3737. [CrossRef]

51. Miao, Q.; Hakimifar, A.; Akbar Razavi, S.A.; Abbasi, H.; Tehrani, A.A.; Chen, J.-Q.; Hu, M.-L.; Morsali, A.; Retailleau, P. Multi-functionalization strategy for environmental monitoring: A metal-organic framework for high capacity Mercury(II) removal and exceptionally sensitive detection of nitroaromatics. *J. Clean. Prod.* **2022**, *376*, 134301. [CrossRef]
52. Pramanik, S.; Zheng, C.; Zhang, X.; Emge, T.J.; Li, J. New microporous metal–organic framework demonstrating unique selectivity for detection of high explosives and aromatic compounds. *J. Am. Chem. Soc.* **2011**, *133*, 4153–4155. [CrossRef]
53. He, Q.; Guan, T.; He, Y.; Lu, B.; Li, D.; Chen, X.; Feng, G.; Liu, S.; Ji, Y.; Xin, M. Digital encoding based molecular imprinting suspension array for multiplexed label-free sensing of phenol derivatives. *Sens. Actuators B Chem.* **2018**, *271*, 367–373. [CrossRef]
54. Kaur, S.; Bhalla, V.; Vij, V.; Kumar, M. Fluorescent aggregates of hetero-oligophenylene derivative as "no quenching" probe for detection of picric acid at femtogram level. *J. Mater. Chem. C* **2014**, *2*, 3936–3941. [CrossRef]
55. Nagarkar, S.S.; Desai, A.V.; Ghosh, S.K. A fluorescent metal–organic framework for highly selective detection of nitro explosives in the aqueous phase. *Chem. Commun.* **2014**, *50*, 8915–8918. [CrossRef] [PubMed]
56. Gong, T.; Li, P.; Sui, Q.; Chen, J.; Xu, J.; Gao, E.-Q. A stable electron-deficient metal–organic framework for colorimetric and luminescence sensing of phenols and anilines. *J. Mater. Chem. A* **2018**, *6*, 9236–9244. [CrossRef]
57. Wen, Y.; Li, R.; Liu, J.; Zhang, X.; Wang, P.; Zhang, X.; Zhou, B.; Li, H.; Wang, J.; Li, Z. Promotion effect of Zn on 2D bimetallic NiZn metal organic framework nanosheets for tyrosinase immobilization and ultrasensitive detection of phenol. *Anal. Chim. Acta* **2020**, *1127*, 131–139. [CrossRef] [PubMed]
58. Li, Z.-H.; Xue, L.-P.; Li, S.; Zang, P.-F. Different metal–ligand ratios regulated two Cd (II)-containing viologen-derived photochromic coordination polymers. *Dye. Pigment.* **2022**, *200*, 110129. [CrossRef]
59. Azhdari Tehrani, A.; Esrafili, L.; Abedi, S.; Morsali, A.; Carlucci, L.; Proserpio, D.M.; Wang, J.; Junk, P.C.; Liu, T. Urea metal–organic frameworks for nitro-substituted compounds sensing. *Inorg. Chem.* **2017**, *56*, 1446–1454. [CrossRef]

Disclaimer/Publisher's Note: The statements, opinions and data contained in all publications are solely those of the individual author(s) and contributor(s) and not of MDPI and/or the editor(s). MDPI and/or the editor(s) disclaim responsibility for any injury to people or property resulting from any ideas, methods, instructions or products referred to in the content.